ELSEVIER

Journal of Process Control 11 (2001) 565–586

JOURNAL OF PROCESS CONTROL

www.elsevier.com/locate/jprocont

Mathematical model for predictive control of the bell-less top charging system of a blast furnace

V.R. Radhakrishnan *, K. Maruthy Ram [1]

Indian Institute of Technology, Kharagpur-721302, India

Abstract

Modern blast furnaces use bell-less top systems for the charging of the solid feed into the furnace. The complete potential of the charging system for distributing the material in the furnace cross-section in any desired profile can be achieved only by using a suitable charge distribution model. By considering the flow of different types of solid particles like iron ore, sinter and coke through the bin and rotating chute, equations have been developed for the particle trajectories. The formation of the ring shaped hill of material by the accumulation of the falling material has been modeled considering the angle of repose, rolling and layer penetration. These relationships have been combined with appropriate corrections for the burden descent and the mixed layer formation to develop the overall geometry of the stock line. The burden charge model has been used in an optimization routine to determine the best charging pattern to transit from an existing stock line geometry to a new geometry. The models have been tested in an operating furnace and incorporated in a supervisory control system.

Keywords: Charging system; Blast furnace; Predictive control; Iron making; Bell-less top

1. Introduction

The blast furnace is the first and often the most critical step in the manufacture of iron and steel. A blast furnace consists of a large vertical furnace. Typically a blast furnace may be 35 m high, with a diameter of 12 m at the largest cross-section and may have a useful volume of about 2100 m^3. Modern blast furnaces have the capacity to produce about 3000 ton/day of hot metal. Accompanied with each ton of hot metal about 0.6 ton of slag and 2500 standard m^3 of gas are produced. The raw material for iron production are iron sources such as ore, sinter and pellets, flux material such as lime stone and dolomite and an energy source which is normally coke. These are charged from the top of the furnace. Tonnage oxygen in the form of enriched air enters the furnace from the bottom. The required quantities of raw materials vary widely. Typical values for producing 1 ton of hot metal are 800 kg coke, 800 kg of ore, 1100 kg of sinter, 40 kg of manganese ore, 90 kg of limestone and 3400 standard m^3 of oxygen enriched hot air blast.

The solid raw material is charged into the blast furnace from the top with the help of skips and a feeding mechanism such as the Paul–Wurth system fitted at the top of the furnace. The material is charged in specified layers of iron bearing material, coke and limestone and the layers move continuously downward. At the bottom of the furnace the hot oxygen enriched air is blasted into the furnace through the tuyeres. The coke in the furnace undergoes partial combustion to produce hot carbon monoxide rich gases which rise up the furnace. The reducing gases rising up the furnace comes into contact with the descending iron ore and reduces it to iron in a series of complex solid–gas–liquid reactions. At the furnace top the material form a free surface with a three dimensional symmetry. Some free board is provided above the free surface of the solids to provide for solid disengagement as well as the required head space for the charging mechanism. Currently the most common charging mechanism is the Paul–Wurth type charging system. The free solids surface at the top of the furnace is known as the stock-line. The initial shape of the stock line has a profound effect on the smooth downward passage of the solids layer.

In a blast furnace the descending solid material comes into contact with the rising hot reducing gases, undergoes a series of complex solid–gas, solid–solid and solid–liquid reactions to produce the molten iron and

* Corresponding author at present address: School of Chemical Engineering, Universiti Sains Malaysia, 31750, Tronoh, Malaysia. Tel.: +60-5-367-6901; fax: +60-5-367-7055.

E-mail address: chradha@kimia.eng.usm.my (V.R. Radhakrishnan).

[1] Present address: Blast Furnace Department, Bhilai Steel Plant, Bhilai, India.

0959-1524/01/$ - see front matter
PII: S0959-1524(00)00026-3

Nomenclature

A	area, m^2
A_p	projected area, m^2
A	acceleration, m/s^2
C_d	drag coefficient
d	diameter, m
e	error, m
E_m	collision energy, J
F	force, N
g	acceleration due to gravity, m/s^2
h_t	height of particle at time t, m
H_d	height of down comer, m
l	longitudinal position, scattering distance, m
L	length of chute, m
L	points on the lower trajectory
L_c	mixed layer thickness, m
M	mass, kg
K_f	correction factor for particle collision
K_1	constant
p	distance,m
r	r-coordinate measured from center line, m
r_c	radius of chute tip, m
R	represents points on stock line
Re	Reynold's number
T	centrifugal force, N
U	points on the upper trajectory
V	velocity, m/s
V_r	volume of material dumped on the rth ring, m^3
V_b	batch volume dumped, m^3
V_c	volume of coke dumped in a batch, m^3
V_{nc}	volume of non-coke dumped in a batch, m^3
Z	z-coordinate measured from the chute pivot, m (Up-ward direction positive)

Greek letters

α	chute angle, rad
β	acute angle between hopper cone and horizontal, rad
η	maximum angle of repose, rad
ϕ	correction factor for braking effect of chute liners, rad
μ	coefficient of friction
μ_g	viscosity of gas, Ns/m^2
ρ	density, kg/m^3
ω	angular velocity, rad/s
θ	angular position, rad
ζ	angle made by the pile with the horizontal, rad
δ	throw angle, rad

Subscripts

b	buoyancy
d	dump, drag
1,2,3	down comer entrance, down comer exit and chute exit respectively
f	frictional
g	gravitational
r,z,θ	radial, z direction and theta direction
g	gas
s	solid
re	relative
p	particle
n−1, n, n+1	position along lower trajectory
i−1,i, i+1	position along stock line
t	tangential
v	vertical
j	ring number, $j = 1..11$
m−1,m,m+1	position along upper trajectory
r	reaction
S,Q,P,T	points ref. Fig. 3

Superscript

b	base
t	target
1,2.	iteration number

slag. Material layering and permeability play important roles in promoting the gas–solid contact and hence the reduction efficiency and throughput of the furnace. Improper layering of material can cause segregation of material, thus reducing the contact efficiency. Non uniform layering of material can also lead to channeling of the material at the periphery as well as to a condition known as the furnace hanging. When furnace hanging occurs the downward movement of the solid material stops. Under this condition the furnace production becomes zero. All these conditions lead to decrease in the furnace productivity.

The blast furnace burden consists of different species of material each of which in turn is a mixture of particles of various sizes and shapes. The coke and non-coke material is charged separately to form distinct layers. Studies [1] have been reported relating the effect of layering during charging with the development of the

profiles during the burden descent in the furnace. These studies have shown that the burden descends cohesively as charged for some distance, till the iron bearing materials are softened and fused. It was further determined that an initial 'V' shape during charging gives rise to an inverted 'V' shaped cohesive zone. This type shape gives the best gas solid contact and furnace productivity.

2. Bell-less top charging system

The conventional twin bell charging systems of blast furnaces have been replaced by the bell-less top charging system first developed in Germany and Austria in the 1970s. The widely used central bin discharge system is schematically shown in Fig. 1.

The solid feed materials are weighed and prepared in bottom bunkers from where they are elevated to the furnace top by skips or conveyors and stored in the receiving hopper, RH. The material is discharged into the feed hopper H as required. The gate valve is used to control the flow rate of solids from the feed hopper. The material falls through the down comer DC that acts as a seal to prevent the gases from escaping. The material then passes to the rotating chute RC. The rotating chute has two degrees of freedom. It can rotate about its axis as well as its angle of inclination with the horizontal can be changed. Hence the r and θ coordinates of the tip of the rotating chute can be changed. The material slides down the chute and after leaving it undergoes free fall in the furnace. The material falls countercurrent to the ascending hot gases till they hit the stock line where they form a ring shaped hill.

The bell-less top charging systems have the following three controls:

1. The rate of flow of material by controlling the opening of the gate valve.
2. The angle of inclination of the chute and hence the radial position on the stock line where the material is charged.
3. The theta coordinate and the speed of rotation of the chute.

These variables are controlled by a PLC system, hydraulic actuators and motor control. With these controls it is possible to charge the material in different ways.

1. Spot charging
2. Ring charging
3. Segment charging
4. Spiral charging

The design data for the bell-less top charging system modeled in this study is shown in Table 1. The chute

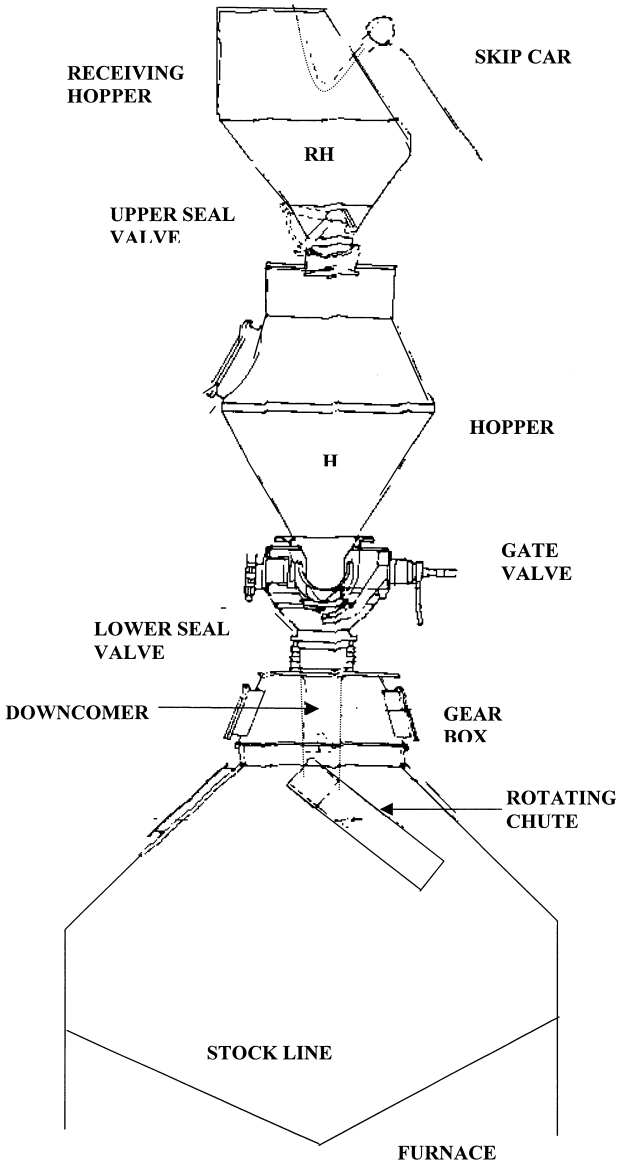

Fig. 1. Bell-less top charging system.

angle could be set at 11 positions corresponding to the values of 16.5–48.5° from the horizontal as shown in Table 2.

To obtain the optimum production of the furnace the charge is to be dumped in certain preferred geometry so as to avoid undesirable conditions like material channeling and 'furnace hanging' taking place. 'Furnace hanging' is a condition where the downward movement of solids stops and furnace productivity becomes zero. A V shaped profile is preferred in most situations. As the material descends this profile is distorted to give a new base line for the next charging. During the next charging an endeavor is made to bring back the profile to the desired geometry. The bell-less top charging equipment has the capacity to charge the material anywhere on the stock line surface. However to bring the

Table 1
Design data of blast furnace bell-less top charging equipment

1	Bin capacity	30 t
2	Type of chute	Fish plate
3	Height of down comer	4.532 m
4	Diameter of down comer	0.75 m
5	Length of chute	3.5m
6	Speed of rotation	8 rpm
7	Reference height of pivot point	+40300 mm
8	Height of maximum operating stock line from chute	−8800 mm
9	Height of minimum operating stock line from chute	−10800 mm
10	Skip capacity	10 m^3
11	Throat radius at operating stock line	3450 mm
12	Stock rod positions	±1950 mm
13	Material charged	Coke, limestone, sinter, ore
14	Number of charges for each dump	2
15	Number of charges per batch	2 coke, 2 non-coke
16	Maximum weight of material per charge	Coke 5T, Ore, sinter 14 T
17	Number of chute settings used per dump	3

Table 2
Chute angles corresponding to charging ring positions

Ring no.	Chute angle, degrees
1	16.5
2	24.0
3	28.0
4	31.5
5	34.0
6	37.0
7	39.0
8	41.5
9	44.0
10	46.5
11	48.5

surface profile from a given base line to a specified geometry requires the use of a mathematical model. This model should be able to predict the shape of the surface after a given amount of material is dumped in a given pattern. Once such a model is available we can formulate and solve the predictive control problem which can be stated as: 'Given a certain base line geometry and the quantity of material available for dumping determine the charging pattern which will take the geometry nearest to the preferred target surface geometry.' The present paper attempts to develop a stock line geometry model from simple mechanistic considerations and to use the model in an optimization program to determine the predictive control algorithm. The design and tuning of the servo control system to implement the supervisory level commands is also discussed.

Some studies on the fundamentals of the flow of material through the bell-less top charging system and the formation of the stock line have been reported in literature. Okumo et al. [2] reported a study on the radial variation of the ore to coke ratio and top surface profiles as a function of charging conditions. This model was the basis of a theoretical model known as RABIT (Radial Burden Distribution Index by Theoretical Model). Burk and Burges [3] coupled the RABIT model with the heat transfer and chemical reaction rates to predict the temperature and gas composition through out the furnace. This model was implemented in a furnace in Port Kembala, but required extensive instrumentation and online data.

Yoshimasa et al., [4] made an extensive study of the particle movement through the bell-less charging system. Their studies gave very important results for later modeling. Some of their important conclusions are,

1. Discharge of material through the hopper is basically by funnel flow.
2. Due to collision forces the particle velocity in the down comer is reduced from the value calculated by the Newton's Law.
3. During discharge in the rotating chute the coarser particles tend to segregate closer to the upper stream.
4. When non-coke material (ore, sinter, pellets) are discharged over a coke layer, they penetrate into the coke layer. The coke layer is transported towards the center line of the furnace. This is called mixed layer formation and can be quantified as a function of impact energy. Sakai et al., [5] in a later study reported that mixed layer formation occurs only in the central region of the furnace. They also determined that the increased coke layer thickness due to the mixed layer formation occurs up to 0.35 R from the center line where R is the furnace radius.

Complete charge modeling and successful online implementation have been reported by Japanese Steel Companies [6] but no details are available.

3. Burden trajectory

The material stored in the hopper falls through the down comer and passes through the rotating chute.After leaving the tip of the rotating chute the particles undergo free fall till they reach the stock-line. Hence, the first part of the model has to determine the particle trajectory through the different parts of the system.

3.1. Assumptions

Following earlier workers [4,5] the model is derived on the basis of these assumptions.

1. Flow of material through the hopper is by funnel flow.

2. At the top of the down comer the horizontal component of the velocity is zero.
3. During the flow through the down comer in-flight collisions reduce the vertical component of the velocity.
4. During sliding flow over surfaces the particle does not leave the surface.
5. Since the density of the rising gases is low compared to those of falling particles and the velocities are low and hence the drag force and buoyancy force may be neglected in comparison to the gravitational forces.
6. The rotating chute can take only certain specified angular positions with reference to the vertical. This lead to material discharge only at certain specified radial ring shaped positions.
7. The chute makes complete integer number of revolutions at each angular position.
8. Mixed layer formation takes place when non-coke material is discharged on a coke layer. When coke is discharged on non-coke material the penetration and mixed layer formation are small and are neglected.
9. The stock-line can be approximated by piece wise linearization.
10. Burden descent is uniform throughout the cross-section of the furnace and is represented by the measured stock rod movement. Stock rods are part of the instrumentation system used for measuring the burden descend rate. The system consists of several plumb line like devices which are lowered on to the surface of the stock-line and held taut by a servo device. The rate of descent of the plumb lines at several locations on the stock line are determined and hence the average stock line descend profile is calculated using a linear approximation.
11. The chute rotates about the centerline and hence the stock line geometry is symmetrical about the centerline.

3.2. Hopper

Yoshimas et al. [7] have presented an equation for the flow of particulate solids through hoppers. They found that the flow rate is substantially independent of the depth of solids in the hopper, provided the material height is at least four times the diameter of the hopper. They also determined that the flow rate is proportional to the effective diameter of the discharge opening raised to the power of 2.5. The effective diameter is defined as the orifice diameter minus the particle diameter. The flow model can be represented by the equation,

$$G = \frac{\pi}{4}\rho_s d_{\text{eff}}^{2.5} g^{0.5}\left\{\frac{1-\cos\beta}{2\sin^3\beta}\right\}^{0.5} \tag{1}$$

where

G = mass flow rate, kg/s;
ρ_s = density of particles, kg/m^3;
d_{eff} = effective diameter of the discharge orifice, m;
g = acceleration due to gravity, m/s^2;
β = acute angle between the cone wall and the horizontal, radian

The velocity V_{1v} at the hopper outlet is calculated from the mass flow rate, bulk velocity and the orifice diameter. The velocity has no horizontal component and has only a vertical component.

3.3. Down comer

The particles fall through the height H_d and are accelerated under the action of gravity. However inter-particle and particle to wall collisions reduce their final velocity from the ideal Newton's Law value. The exit velocity from the down comer is given by

$$V_{2v} = \left[V_{1v}^2 + 2g_{H_d}\right]^{0.5} K_f \tag{2}$$

V_{1v}, V_{2v} = velocity at the entrance and exit of the down comer, respectively, m/s
H_d = height of down comer, m
K_f = correction factor for collisions

3.4. Revolving chute

The particle falling on the revolving chute RC (Fig. 2) is acted upon by [8]:

1. Frictional Force F_F—parallel to the chute surface.
2. Gravitational force mg—vertically downwards.
3. Centrifugal force F_T—in tangential direction.
4. Reaction F_R—perpendicular to the chute.

Resolving the forces perpendicular to the chute surface,

$$F_R = mg\cos\alpha - m_\omega^2 r\sin\alpha; \tag{3}$$

α = angle of inclination of chute to horizontal radians (Fig. 2.);
ω = angular velocity, radian/s;
m = mass of the particle, kg;
F_R = reactive force perpendicular to the chute, N.

Similarly, resolving the forces parallel to the surface we get the frictional force F_F as,

$$F_F = m_\omega^2 r\cos\alpha + mg\sin\alpha \tag{4}$$

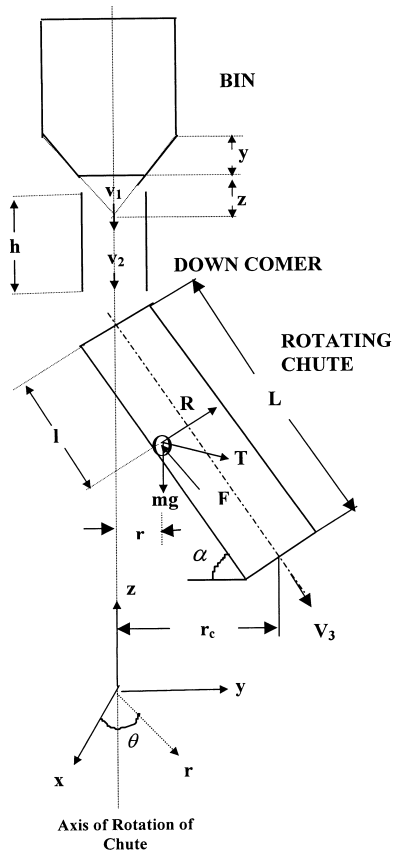

Fig. 2. Flow of solid particles through the system.

r = radial position of the particle from the center, m (Fig. 2)
F_F = Frictional force, N.

With $r = l\cos\alpha$ and acceleration $a = d^2l/dT^2 = v(dv/dl)$ a force balance along the direction of the chute yields,

$$mV\frac{dV}{dl} = m_\omega^2 l\cos\alpha(\cos\alpha + \mu\sin\alpha) + mg(\sin\alpha - \mu\cos\alpha) \quad (5)$$

l = longitudinal position of the particle, m (Fig. 2);
μ = Coefficient of friction between the particles and the chute surface.

The exit velocity of the particle as it leaves the chute is given by integrating Eq. (5) over the length of the chute that is $l = 0$ to $l = L$. Integrating with the limits $l = 0$, $V = V_{2v}\sin\alpha$; $l = L$, $V = V_3$, we get the velocity along the chute at the exit as,

$$V_3 = [\omega^2\cos\alpha(\cos\alpha + \mu\sin\alpha)L^2 + 2g(\sin\alpha - \mu\cos\alpha)L + (V_{2v}\sin\alpha)^2]^{0.5} \quad (6)$$

The particle to chute friction coefficient μ depends on the type of material and the chute surface. In practice, the chute surface is lined with wear resistance plates of different kinds such as fish plates and ribbed plates. Nagai [9], has reported that these surfaces exert a large braking force on the particles. Nagai [9], accounted for the braking effect by a correction factor ϕ. This factor ϕ is defined as the actual distance on the chute surface over which the particle slides divided by the length of the chute. They found that the length L in Eq. (6) should be the actual length of sliding and not the chute length. The value of the correction factor depends on the type of surface lining on the chute as well as the angle of inclination of the chute. The value of ϕ varies between 1 for a nearly vertical chute to 0.948 for a chute angle of 42.5 degrees. These values were experimentally determined for various chute angles and is reported in Table 6. Hence, by replacing the chute length L by the effective chute length $L\phi$ we get,

$$V_3 = [\omega^2\cos\alpha(\cos\alpha + \mu\sin\alpha)L^2\phi^2 + 2g(\sin\alpha - \mu\cos\alpha)L\phi + (V_{2v}\sin\alpha)^2]^{0.5} \quad (7)$$

The velocity V_3 along the chute can be resolved in the radial, vertical and tangential directions to give,

$$V_3 = V_3\cos\alpha;$$
$$V_z = -V_3\sin\alpha; \quad (8)$$
$$V_\theta = r_c\omega.$$

where r_c is the radius to the tip of the chute.

For high values of ω and $\alpha > \pi/4$ the reaction F_R [Eq. (3)] can become negative and hence the particles may lift off from the chute surface. For large values of α the chute is nearly vertical, and the main force acting on the particle is the gravitational force mgsinα leading to free fall of the particle. For small values of α, with the chute nearly horizontal the force parallel to the chute [Eq. (5)] becomes large and the particle is accelerated towards the chute tip by the continuously increasing centrifugal force.

3.5. Trajectory of the particle in the freeboard

After leaving the chute tip with vertical, radial and tangential components of the velocity the particle undergoes free fall till it strikes the stock line. The forces acting on the particle during the fall through the gaseous medium are the gravitational force, buoyancy force and the drag force. Since the density of the blast furnace gas is small compared to the particle density the buoyancy forces can be neglected. For the particles used in the charge which are fairly large in size the drag force is mostly caused by the form friction. The gas velocity being small compared to the particle velocity we can consider the relative velocity to be equal to the particle velocity.

3.6. Radial coordinate

Since the particle velocity has three components as given in Eq. (8) the drag force can also be resolved in the three directions. The horizontal component of the drag force acting in the radial direction is constant through out the trajectory and has a relatively small magnitude. Hence it can be neglected. With these assumptions the velocity of motion in the r direction can be written as,

$$m\{\frac{\partial^2 r}{\partial_t^2} - r[\frac{\partial\theta}{\partial t}]^2\} = 0 \tag{9}$$

with

$$r = \sqrt{r_c^2 + 2r_c v_r t + v_r^2 t^2 + v_\theta^2 t^2}$$

Integrating the equation twice with the boundary conditions $t = 0$, $r = r_c$ and $dr/dt = V_r = V_3 \cos\alpha$ gives the radial position of the particle at time t.

$$r = r_c + (V_3 \cos\alpha)t + \frac{V_\theta^2 t^2}{2_{r_0}} + \text{cubic term in } t \tag{10}$$

t = time after leaving chute tip, s;
r_c = radius of chute tip, m.

For small time intervals the equation may be further simplified by considering only the linear terms as

$$r = r_c + (V_3 \cos\alpha)t \tag{11}$$

3.7. Tangential coordinate

The tangential force acts tangentially to the circle made by the chute tip in the r, θ plane. Since we can reasonably assume that the stock line geometry to be symmetrical about the centerline, the θ coordinates are not required for the model.

3.8. Vertical coordinate

The vertical coordinate of the particle can be determined in the same way by writing the force balance in the z direction. The forces acting on the particle are the vertical component of the drag force and the gravitational force. Neglecting the drag force the equation of motion can be written as

$$\frac{d^2 z}{dt^2} = -g \tag{12}$$

Integrating Eq. (12) with the initial condition $t = 0$, $(dz/dt) = -V_3 \sin\alpha$

$$\frac{dz}{dt} = -gt - v_3 \sin\alpha \tag{13}$$

Integrating Eq. (13) with the initial condition $t = 0$, $z = z_c$ where z_c is the z coordinate of chute tip

$$z = \frac{-gt^2}{2} - (v_3 \sin\alpha)t + z_c \tag{14}$$

The height through which the particle falls during its free fall and the time of flight are related by the equation of motion

$$h_t = v_3 t + \frac{gt^2}{2} \tag{15}$$

from which the time of flight can be written as

$$t = \frac{\{-v_3 \pm (v_3^2 + 2gh_t)^{0.5}\}}{g} \tag{16}$$

Eqs. (11) and (14) can be used to determine the r and z coordinates of the trajectory of the particle for any time t from $t = 0$ to the time the particle hits the stock line as given in Eq. (16).

4. Stock line geometry

The descending material is confined within an upper and lower boundary as shown in Fig. (3) When the descending material reaches the stock line it forms a ring shaped hill due to the rotation of the chute about its axis. Depending on the method of charging, the material may form either a single ring or multiple rings with or without overlapping. These concentric ring-shaped hills of material constitute the new surface profile

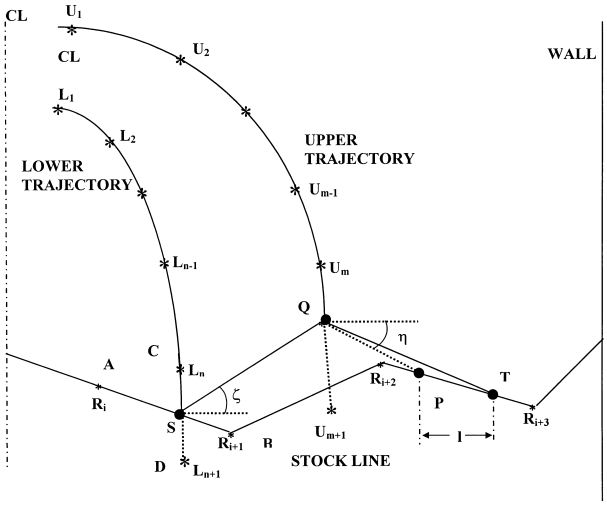

Fig. 3. Trajectory of particles in the freeboard and stock line formation.

after a charging sequence. The shape of the hill (in elevation) are governed by various factors like the speed of revolution of the chute, the rate of discharge of material, the coefficient of rolling friction and the angle of repose. Another factor, which governs the shape, is whether the discharge is of a heavy material into a bed of softer material or vice versa. In the former case the heavy material can penetrate the bed thus distorting the shape and forming a mixed layer. A model for the stock line geometry is derived taking into account these factors.

Since the material leaves the chute with radial and tangential velocities the tendency of the material is to roll and settle outwards towards the wall. Because of this tendency the hill of material can be assumed to start building up from the point of inner boundary at an angle which may be less than the maximum angle of repose. If any rolling takes place it has to be outwards due to the radial velocity. When the material builds up and reaches the maximum angle of repose then there could be rolling towards the center of the furnace. Because of this we can start the build up of the hill from the point of intersection of the lower trajectory with the stock line.

The solids build up on the stock line is analyzed on the basis of the following assumptions.

1. The chute rotates at a uniform speed and hence the ring is symmetrical about its center.
2. The number of rotations of the chute in any ring is an integer.
3. The chute can take only certain specified angular positions (Table 6).

4.1. Point of intersection of the lower and upper boundaries of the falling material with the stock line

The material falling on the stock line starts to accumulate and finally takes the shape of a hill. The flow of material as shown in Fig. 3 is bounded by a lower and an upper boundary or trajectory.

The upper trajectory is defined by a series of points denoted U_m, the lower trajectory denoted by a series of points denoted L_n and the stock line denoted by a series of points denoted R_i. Each of these points has an r and z coordinate. These trajectories are modeled using a piece wise linearization approach. As discussed earlier the θ coordinate need not be considered because of the axial symmetry assumed. Assuming that the material builds up from the contact point of the lower trajectory with the base stock line (Fig. 3) we can determine the point of intersection S of the lower trajectory with the base stock line. As shown in Fig. 3, S is the point of intersection of the line CD with the line AB. The trajectory CD though a parabola, can be approximated by the straight line CD. Similarly the surface profile is approximated by the straight line AB. Since the r and z coordinates of point A,B, C and D are known we can write the equations for the straight lines AB and CD in the form, $z = mr + c$. The coordinate of the point S (r_s, z_s) is given by the intersection of the straight lines AB and CD.

The material falling between the lower and upper boundary after being deposited on the stock line forms into a heap. As explained earlier the buildup of the material is from the point of intersection of the lower trajectory with the existing stock line, so long as the angle of repose is less than the maximum angle of repose. Hence material is assumed to buildup from the point S (Fig. 3) along the line SQ. We assume that the surface of the built up material forms an angle ζ with the horizontal where ζ is an assumed angle of repose. The trial value of the angle ζ is chosen at a value lower than η the maximum angle of repose for the material. The volume of the hill so formed should be equal to the dumped volume as discussed in the next section and this is used to iteratively determine the correct value of ζ. The line SQ has the equation

$$z = r\tan\varsigma + z_s - r_3\tan\zeta \tag{17}$$

The equation of the line connecting the points U_m, U_{m+1} on the upper trajectory can be approximated by a straight line. The point of intersection of the upper trajectory with the stock line SQ is given by the coordinates

$$r_Q = \frac{c - z_s + r_s\tan\zeta}{\tan\varsigma - m} \tag{18a}$$

$$z_Q = r_Q\tan\zeta + z_S - r_s\tan\zeta \tag{18b}$$

4.2. Construction of the new stock line profile

The material falling on the stock line rolls and spreads beyond the upper trajectory because of the radial and tangential velocity components. This outward scattering is defined by a scattering distance. The closing boundary of the material after settling lies between the upper trajectory and the wall on the old stock line or it may lie on the furnace wall itself. Kajimasa et al. [6] in their study suggested that material filling towards the wall rests at the maximum angle of repose. Hay et al. [10] determined that the scattering distance for coke and non-coke materials are essentially constant and have average values of 0.7 and 0.5 m, respectively. Using these findings a procedure has been developed for determining the outer boundary T of the hill of material between the upper trajectory and the wall. At point Q a line QP is constructed at an angle η, the maximum angle of repose to the horizontal. The equation of the line QP can be written as

$$(z - z_Q) = \tan\eta(r - r_Q) \tag{19}$$

P is the intersection of the line QP with the line $R_{i+2}R_{i+3}$. The coordinate of the point P (z_p, r_p) can be obtained by solving the Eq. (19) with the equation of the line joining the points (z_{i+2}, r_{i+2}) with (z_{i+3}, r_{i+3}). The coordinates of the point P are given as

$$r_p = \frac{-\tan\eta r_Q + z_Q + \dfrac{(z_{i+3} - z_{i+2})}{(r_{i+3} - r_{i+2})} - z_{i+2}}{-\tan\eta + \dfrac{(z_{i+3} - z_{i+2})}{(r_{i+3} - r_{i+2})}} \tag{20a}$$

$$z_p = -r_Q \tan\eta + z_Q - r_p \tan\eta \tag{20b}$$

The material hitting the stock line at point P rolls through a distance l outwards and settles at point T. This distance called the scatter length was measured experimentally using a cold model of the rotating chute system. It was found that all iron bearing material and limestone had a scatter length of 0.5 m and the coke had a scatter length of 0.75 m (Table 3) for the range of particle velocities encountered in the model. The coordinates of the point T can be obtained by adding the scatter length as

$$r_T = r_p + l \tag{21a}$$

$$z_T = z_p + \frac{z_{i+3} - z_{i+2}}{r_{i+3} - r_{i+2}} l \tag{21b}$$

The coordinates of the points S, Q and T define the cross-section of the ring of material formed by the discharge of material from the chute.

4.3. Calculation of the volume of material in the ring shaped hill

The cross-section of the hill is a polygon bounded by the sides SQ and QT together with the old stock line given by $SR_{i+1}R_{i+2}T$. The volume of the ring of material is calculated using standard methods of mensuration.

Table 3
Properties of burden charge

	Coke	Ore + sinter
Bulk density, t/m^3	0.55	1.86
Hopper discharge flow rate, t/min	16	47
Coefficient of friction	0.6	0.5
Fractional filling of chute	0.57	0.47
Scattering length, m	0.75	0.5
Maximum angle of repose, degree	38.9	39.9

5. Iterative procedure

5.1. Convergence

In an actual operating bell-less top charging system the speed of rotation of the chute is fixed. The flow rate of material is also fixed by controlling the position of the gate valve. Hence the total quantity of material dumped in one ring is known. The calculated value of the volume of rotation of the ring shaped hill should therefore be equal to the volume actually dumped in the ring. If the calculated ring volume agrees to the dumped volume to within 2.5% it has been assumed that the calculation has converged. This condition is used as the convergence criteria given as

$$\frac{|\text{calculated volume} - \text{dumped volume}|}{\text{dumped volume}} \times 100 \leqslant 2.5 \tag{22}$$

We start the iteration assuming that the inner boundary of the ring of material is fixed at the point of contact of the inner trajectory with the stock line S. This essentially means that there is no increase in height at the point S. Cold run experiments conducted with a rotating chute has shown that this assumption is reasonably valid at values of chute angle higher than 15° and speed of rotation of chute higher that 7 rpm. These conditions are satisfied in the range of this model. We further assume, as the starting point of the iteration, that the hill makes an angle of repose equal to ζ which is selected at a trial value less that the maximum angle of repose η. With these conditions the shape of the hill is uniquely fixed by the procedure discussed and its volume can be calculated. The calculation of the ring volume may result in one of the three conditions,

a. the calculated volume is equal to the dumped volume within the allowable tolerance;
b. the calculated volume is less than the dumped volume;
c. the calculated volume is more than the dumped volume.

In the first case convergence has been reached. For the second and third conditions corrections are applied to the boundaries of the ring and the volume recalculated till convergence is attained. The closing boundary of the hill QT is defined by the maximum angle of repose and the scattering distance and hence is not subject to modification. However the inner boundary of the hill can be modified. The angle of repose may have a value higher than the angle chosen for the first iteration, ζ. Let this new angle be $\zeta_1 > \zeta$ with the condition that the angle selected $\zeta_1 < \eta$, where η is the maximum angle of repose of the material. Once the angle of repose has reached its maximum value η the material also can roll

towards the center of the furnace in which case the starting point of the inside boundary will no longer be S but a point towards the center. We can therefore manipulate these two variables, angle of repose and the starting point of the hill, to achieve convergence between the calculated and dumped volumes

When the calculated ring volume is less than the dumped volume of material, for convergence the ring volume must be made larger. Since the outer boundary TQ is decided by the maximum angle of repose and the scatter length, the point T is not subject to manipulation. In this case the only way the ring volume can be higher is for the angle of repose chosen ζ should take a higher value. Therefore the angle ζ is increased in steps of 1° and the procedure explained in the previous section repeated and the ring volume recalculated. If the ring volume is still lower than the dumped volume then the angle is increased further in steps of 1° till it becomes equal to the maximum angle of repose η. If the ring volume is still lower than the dumped volume then the angle cannot be increased further since we have reached the maximum angle of repose. Under such circumstances the only possibility is that the hill does not start from the point S (Fig. 3) but has rolled toward the center of the furnace. It is obvious that rolling towards the center can take place only when the angle has reached the maximum angle of repose. Under these circumstances further increase in the ring volume is obtained by shifting the point S upward along the inner trajectory to the point U as shown in Fig. 4. The hill starts from the point I on the stock line and it makes an angle η (now the maximum angle of repose) with the stock line. The equation of the line UI is given by

$$z = r\tan\mu + z_u - r_u\tan\mu \tag{23}$$

The geometrical shape of the hill of material is represented by IUQT. The volume of material is again

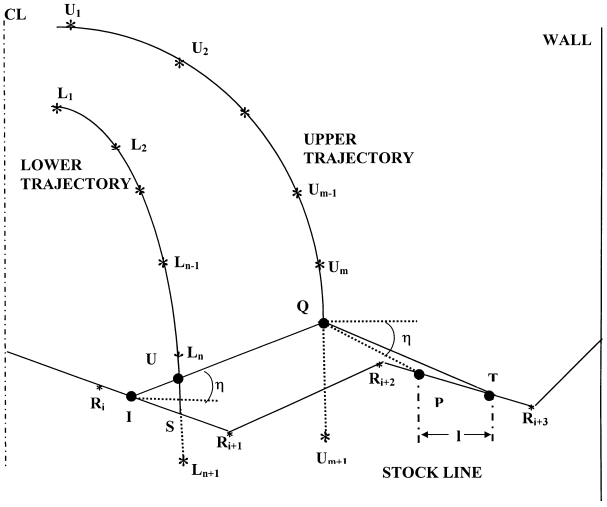

Fig. 4. Convergence procedure for stockpile volume.

calculated and compared with the dumped material. If the volume of the hill calculated is still lower that the dumped volume, then the point U is shifted further upwards along the lower trajectory. An iterative solution is obtained by using a one-dimensional Fibonnaci search till the convergence is obtained.

When the calculated ring volume is higher than the dumped volume then the procedure is to reduce the angle of repose assumed, ζ. In this case the heap makes a smaller angle with the horizontal than assumed. The angle in reduced by one degree and the ring volume recalculated and compared with the dumped volume. An iterative solution is obtained using a Fibonnaci search method till the calculated ring volume agrees with the dump volume to the required tolerance.

6. Correction to the stockline profile for the furnace dynamics

In an actual operating furnace the stock line profile calculated according to the model presented needs correction because of two factors. These are (1) mixed layer formation [6,7] and (2) burden descent [7]. It has been reported [6,7] that when a heavier material like ore or sinter is dumped on an existing stock line made up of a lighter material like coke, then due to the impact energy the coke is scooped out and is transported towards the center of the furnace. This lead to the formation of a region in the center of the furnace consisting of mixed coke-non coke material. Mixed layer formation does not occur when a lighter material is dumped on a denser material. These workers have presented equations to relate the thickness of the mixed layer L_c with the collision energy E_m.

$$L_c = 3.49\times10^{-4}\times E_m - 136 \tag{24}$$

The collision energy is defined as the kinetic energy of the particles at the point of impact and is summed over all the particles.

$$E_m = \sum_{i=1}^{n}\frac{m_i V_i^2}{2} + m_i g H \tag{25}$$

where the summation is over particles of all diameters in the dump.

From the position of the chute, the operating stock line and the particle size distribution the increase in coke layer thickness can be calculated using Eqs. (24) and Eqs. (25). It has been reported by Kajimasa et al. [6] that the increase in coke layer thickness occurred up to a distance of 0.36 times the radius of the furnace from the centerline and that this distance is independent of the furnace size. In the present study, whenever a non coke dump is made on a coke base line the coordinates

of the base stock line up to a distance of 3.5 m from the center line has been corrected for the increase in the coke layer thickness and mixed layer thickness using the Kajimasa et al. [6] model.

The second dynamic effect for which the simulation model needs correction is the burden descent. The burden descent in an operating furnace is measured by using stock rods. These are simple plumb line devices, which are positioned on either side of centerline at fixed distances. Periodically the stock rods are introduced into the furnace and the stock line position and rate of descent measured using a servo system. From this data the average rate of descent of the stock line is available. It is assumed that the whole stock line descends at a uniform rate, which is true for properly operating furnaces. This information is used to correct the position of the stock line from the position corresponding to the previous iteration.

7. Model verification

The two major elements of the model, the particle trajectory and the stock line profile were tested by measurements in a blast furnace. Two types of measurements were performed (a) measurements while the blast furnace was initially filled with charge before being lighted up and (b) measurements on an operating furnace. Measurements on a cold furnace while being filled were relatively easy to perform and several parts of the model could be verified under such measurements. The measurements in an operating furnace were severely limited because of the high temperature and other operational problems. However, for verifying the effect of the furnace operational dynamics such measurements were necessary.

The major dimensions of the furnace charging system (Paul–Wurth bell-less charging system) for which the model was verified is shown in Table 1. The chute could be positioned at 11 positions. The angles corresponding to these positions are shown in Table 2 which also shows the loss factor for the different angles. The properties of the different burden material charged are shown in Table 3. A typical charging pattern in a campaign is shown in Table 4.

7.1. Trajectory

The particle trajectory predicted by the model [Eqs. (11), (14) and (15)] was verified by experiments conducted during the filling of the furnace. A special probe was constructed to measure the radial coordinates of the trajectory at different z coordinates. The probe consisted of a heavy metallic section, which could be introduced into the furnace through manholes available at several positions in the furnace above the stock line. Manholes were available at -6.8, -8, -12, -18 and -25 m with reference to the chute pivot. The probe was covered with a thick coating of chalk dust and then introduced into the furnace and clamped into position. The chute was fixed at a particular angle corresponding to one of the eleven available positions and the discharge of material started. When the material falls over the chalk coated probe the chalk coating is worn off in the region where the material strikes the probe. After some time the material flow is stopped. By measuring the distance over which the chalk is worn off the position of the lower and upper trajectories at the vertical position corresponding to the manhole can be determined. By repeating this experiment at several manhole positions, the trajectory could be measured. These experiments were conducted for both the coke and non-coke material for all the 11 chute angle settings available. Typical results for the discharge of coke at ring setting of 4 and for non-coke material at ring setting of 6 are shown in Fig. 5 and 6, respectively. The experimental conditions corresponding to these tests are summarized in Table 5.

Table 4
Typical charging pattern

Skip no.	Material charged	Weight	Discharge pattern ring numbers
1–2	Coke	9.2	4,5,6
3–4	Non-coke	26.1	4,5
5–6	Coke	9.2	4,5,6
7–8	Non-coke	26.1	4,5
9–10	Coke	9.2	2,3,4
11–12	Non-coke	26.1	4,5
13–14	Coke	9.2	3,4,5
15–16	Non-coke	26.1	4,5
17–18	Coke	9.2	4,5
19–20	Non-coke	26.1	4,5,6

In all the experiments it was observed that the measured values followed the model closely in the case of the upper trajectory. However in the case of the lower trajectory it was observed that the experimental boundary was lower than the boundary predicted in the model. Photographic examination of the discharge from the chute revealed that the solids do not leave the lower lip of the chute tangentially. It was found that the solids make an additional angle with the chute. This additional angle was named δ the throw angle. One possible reason for the throw angle is the bending of the stream due to the Bernouli effect at the lower lip of the chute, similar to liquid pouring out of a vessel adhering to the vessel at the lower trajectory. It was determined that the throw angle was essentially the same for both coke and non coke material and varied between 9 and 14° depending on the chute angle. The throw angles corresponding to the different chute angles are shown in Table 6. Since the particles do not leave the chute at the lower lip tangentially corrections are introduced in the

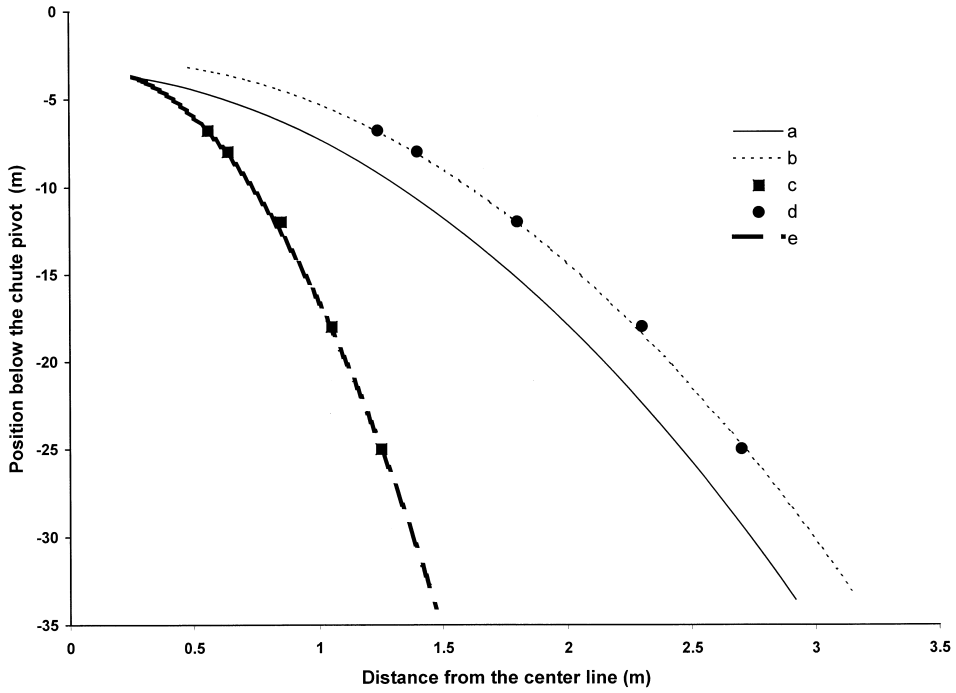

Fig. 5. Model–experiment comparison of trajectory for dumping of coke at a chute angle setting of 23.5° at ring 4 position. (a) Initial model prediction for lower trajectory, (b) model prediction for upper trajectory, (c) measured points in the lower trajectory, (d) measured points in the upper trajectory, (e) model prediction for the lower trajectory after applying correction for throw angle.

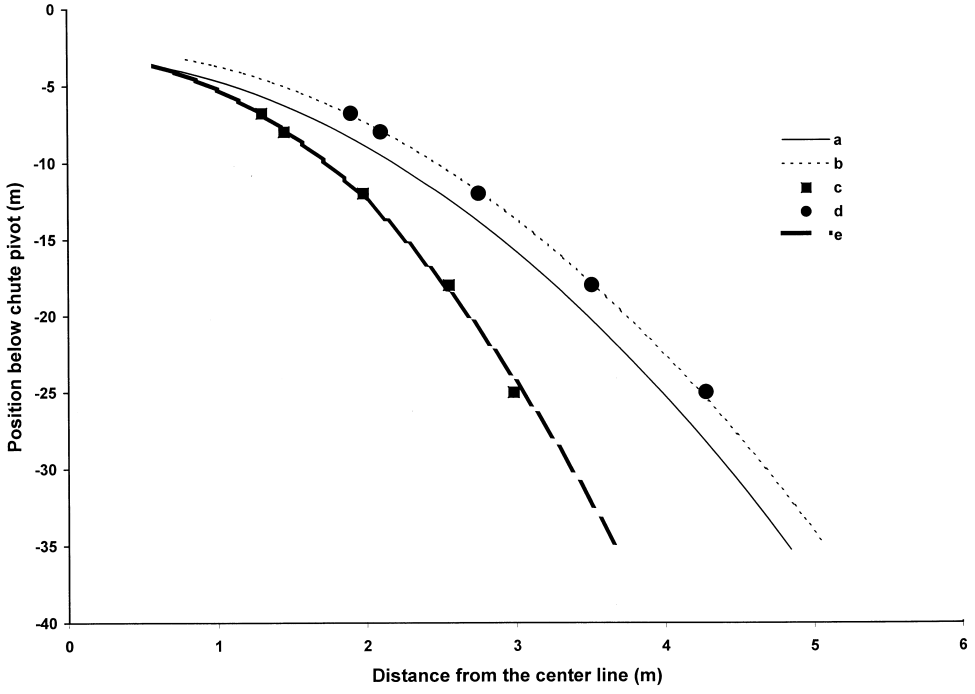

Fig. 6. Model–experiment comparison of trajectory for dumping of non-coke material at a chute angle setting of 28.5° at ring 6 position. (a) Initial model prediction for lower trajectory, (b) model prediction for upper trajectory, (c) measured points in the lower trajectory, (d) measured points in the upper trajectory, (e) model prediction for the lower trajectory after applying correction for throw angle.

Table 5
Experimental conditions for verification of trajectory model

Dumping position			Calculated velocity, m/s		
Ring no.	Chute angle, degrees	Material dumped	Hopper exit	Down comer exit	Chute exit
4	23.50	coke	0.01	3.03	3.77
6	28.50	non-coke	0.01	3.77	4.06

Table 6
Throw angles

Ring no.	Chute angle	Throw angle	Correction factor, ϕ
1	12.0	9.0	1.00
2	18.5	10.0	1.00
3	20.5	10.5	0.98
4	23.5	11.0	0.975
5	25.2	12.0	0.970
6	28.5	12.5	0.965
7	33.0	13.0	0.955
8	35.0	14.0	0.955
9	38.0	14.0	0.950
10	40.5	14.0	0.948
11	42.5	14.0	0.948

angle. Eqs. (11) and (14) for the r and z coordinates of the lower trajectory are modified to give

$$r = [V_3 \cos(\alpha + \delta)t] + r_c \tag{26}$$

$$z = \frac{-gt^2}{2} - [v_3 \sin(\alpha + \delta)t] + z_c \tag{27}$$

With the lower trajectory modified by the inclusion of the throw angle the model-experimental comparison is shown in Fig. 5 curve (e) and Fig. 6 curve (e) for a typical coke and non-coke dump, respectively. With the addition of the throw angle the model is able to closely track the actual trajectory of the material in the furnace.

7.2. Solid profile in the furnace after dumping

The model represented by Eqs. (17) to (27) together with the iterative procedure and convergence conditions constitute the scheme for calculating the stock line geometry after a dump. To test the validity of the model two types of tests were conducted.

1. Cold tests on the furnace during the initial charging.
2. Hot tests on the operating furnace.

For both the series of experiments the set of actual dumping practices as given in Table 4 were simulated by the model and compared with the actual measurements. In the cold run the measurements were obtained by actually measuring the profile using the fish line depth-measuring instrument after the completion of the dump. Curve (a) of Fig. 7 is the base profile and is a coke layer. Curve (b) shows the model predictions when 22.2 ton of sinter + ore are dumped in rings 5,6 and 8 in equal volumes. The measured values of the profile compares very well with the model predictions. Subsequent dumping of 9.2 ton of coke on rings 4,5 and 6, and a second dumping of 22.2 ton of ore + sinter on rings 5,6 and 8 are also illustrated in the figure. Further dumping of a series of different materials and rings are shown in Figs. 8 and 9. The baseline (a) of Fig. 8 is the last dumping profile line (f) of Fig. 7. Similarly line (h) the last profile in Fig. 8 makes the base line (a) of Fig. 9.

In all the cases the model has been able to predict the stock line profile after dump to sufficient accuracy. The standard deviation between the predicted and actual values of the stock line shown in Table 7 is a measure of the accuracy of the model.

Tests were also conducted on the operating furnace to determine the prediction accuracy of the stock line model. In these hot tests thermal imaging was used to determine the actual stock line profile. In Fig. 10 the results of a dump of 26 tons of ore + sinter on a coke baseline is presented. The measured thermal image values agree remarkably well with the predicted data. The standard deviation in this was 0.07 m. Fig. 11 shows the result of coke dump of value 9.2 tons on rings 4 and 5. The baseline was non-coke. In this case also the model is able to predict the profile very accurately the standard deviation being 0.09 m.

8. Predictive control

The primary objective of the predictive control of the bell-less top charging system is to maintain an existing stock line geometry or to transit from a given stock line geometry to a new predefined geometry. This objective can be stated as

Given

1. The present stock line geometry.
2. Target stock line geometry.
3. Amount of charge, coke and non-coke.

Determine the dumping strategy consisting of

1. Ring numbers on which dumping is to take place.
2. Quantity of material dumped in each ring.

The predictive control algorithm can be defined as an error minimization algorithm. The error between the stock line after dump and the target stock line is minimized by manipulating the dumping positions and quantities subject to constraints.

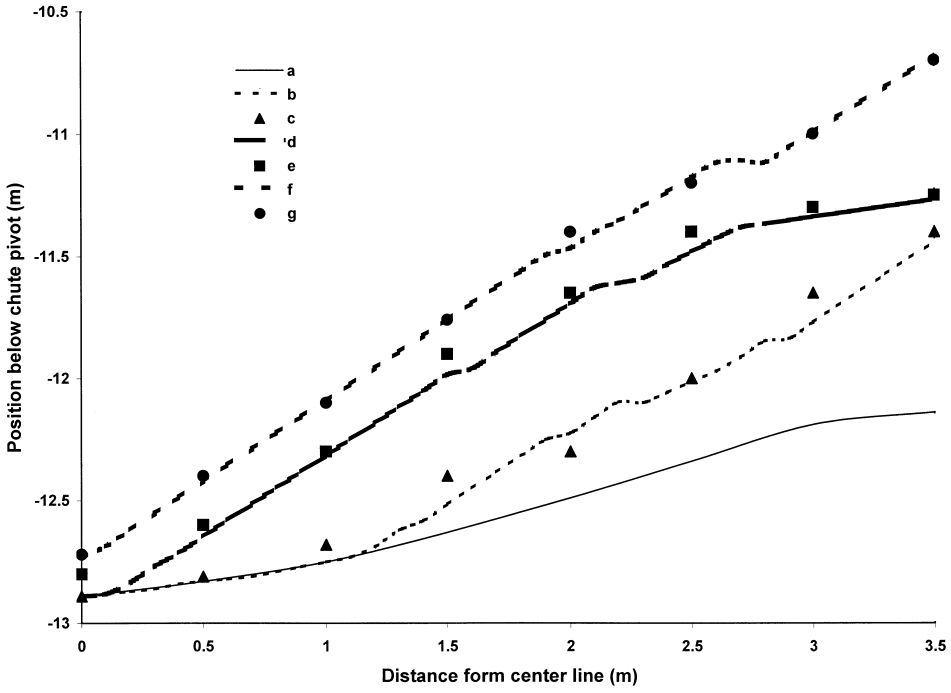

Fig. 7. Model–measurement comparison of stock line geometry after dumping: (a) Base line made up of coke, (b) predicted stock-line after a dump of 22.2 tons of sinter + ore on rings 5,6,8, (c) measured points for the dump, (d) predicted stock line after a coke dump of 9.2 tons on rings 4,5 and 6, (e) measured points for the dump, (f) predicted stock line after a dump of 22.2 tons of sinter + ore on rings 5, 6 and 8, (g) measured points for the dump.

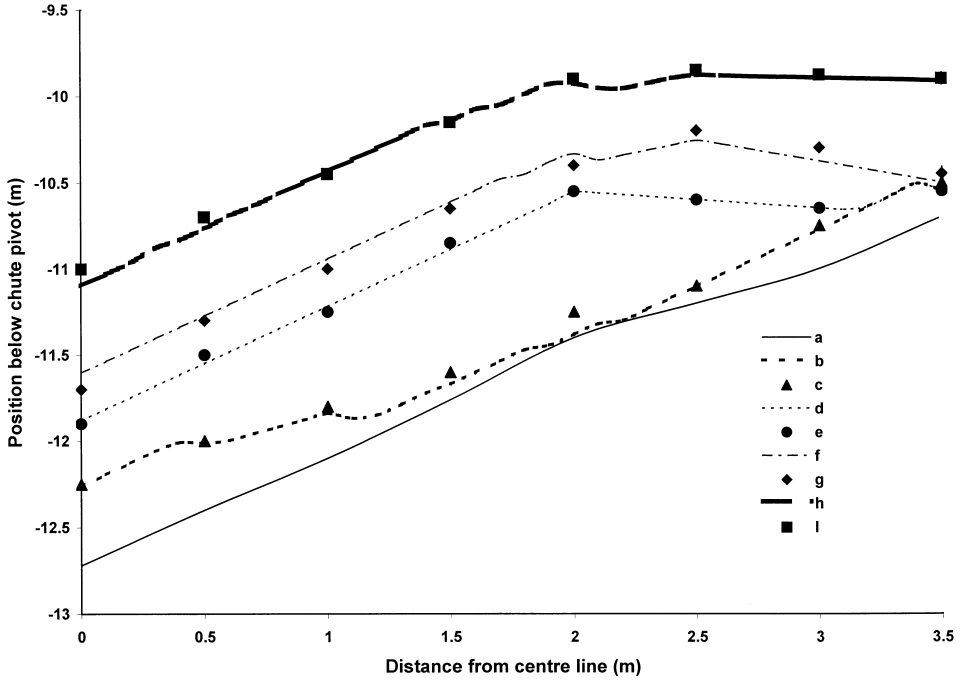

Fig. 8. Model–measurement comparison of stock line geometry after dumping: (a) Base line made up of non-coke material, line (f) of Fig. 7, (b) predicted stock line after a dump of 22.2 tons of sinter + ore on rings 4 to 11, (c) measured points for the dump, (d) predicted stock line after a coke dump of 9.2 tons on rings 4 and 5, (e) measured points for the dump, (f) predicted stock line after a dump of 17.3 tons of sinter on rings 5 and 6, (g) measured points for the dump, (h) predicted stock line after a dump of 10 tons of coke on rings 4,5 and 6, (i) measured points for the dump.

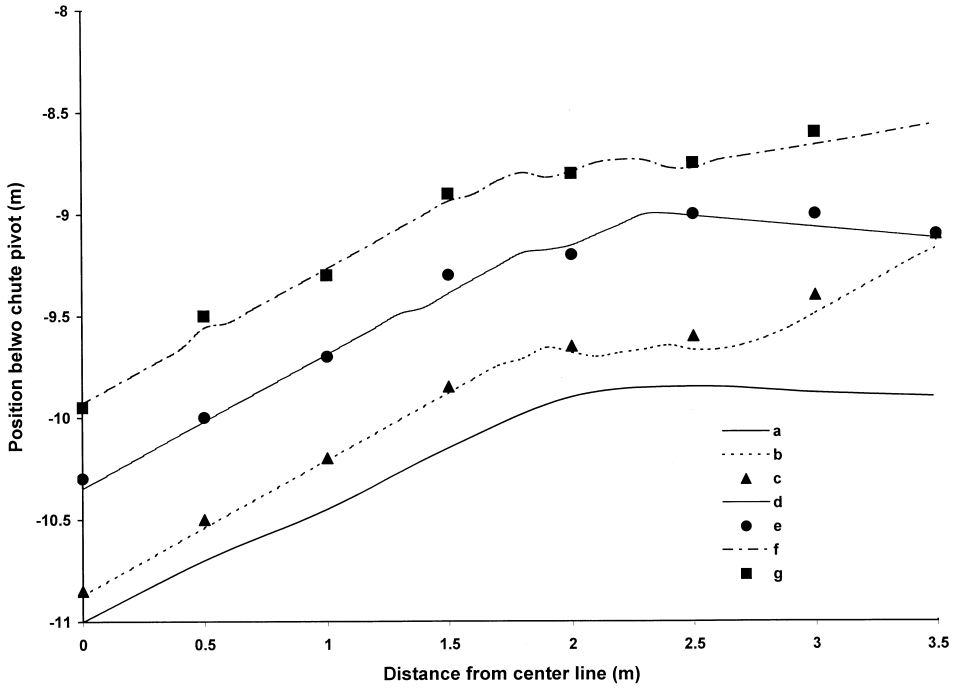

Fig. 9. Model–measurement comparison of stock line geometry after dumping: (a) Base line made up of coke, line (h) of Fig. 8, (b) predicted stock line after a dump of 24.6 tons of sinter on rings 4 to 9, (c) measured points for the dump, (d) predicted stock line after a coke dump of 10.0 tons on rings 4,5 and 6, (e) measured points for the dump, (f) predicted stock line after a dump of 28.07 tons of sinter + ore + limestone on rings 4 to 8, (g) measured points for the dump.

8.1. Optimization algorithm

The optimization algorithm can be formulated as

$$\text{minimize} \qquad \text{Error square} = \sum_{j=1}^{n} e_j^2 \tag{28}$$

$$\text{where} \qquad e_j = z_j^t - z_j \qquad j = 1, 2 \ldots 11 \tag{29}$$

$$\text{Subject to} \qquad z_j^b,\ z_j^t,\ V_c,\ V_{\text{NC}} \quad \text{are specified}$$

The variables available for manipulation are the ring numbers used for dumping, j: $j = 1, 2 \ldots 11$ and the quantity of material dumped in the jth ring, $(V_c + V_{nc})_j$.

Table 7
Standard deviation between model and measured stockline profiles — cold runs

Layer No	Material	Standard deviation
1	S+O	0.11
2	C	0.09
3	S+O	0.07
4	S+O+L	0.05
5	C	0.09
6	S	0.17
7	C	0.15
8	S	0.05
9	C	0.07
10	S+O+L	0.17

The stock line is divided into 11 areas corresponding to the 11 dumping rings. The area of the first ring is $A_1 = \frac{\pi r_1^2}{2}$. The remaining areas are donut shaped and have area of

$$A_j = \frac{\pi(R_j^2 - R_{j-1}^2)}{2} \qquad j = 2, 3 \ldots 11.$$

At the center of each of the 11 areas the vertical distance between the targeted profile and the base profile is determined as

$$d_j = z_j^t - z_j^b \quad j = 1, 2 \ldots 11 \tag{30}$$

The contained volume in the space of base area A_j and bounded by the base and new stock line profiles is given by

$$V_j = A_j \times d_j \quad j = 1, 2 \ldots 11 \tag{31}$$

Hence the total material needed to fill up the space between the base stock line and the target line is given by ΣV_j where the summation is over all the eleven volume elements. The volume of material charged in the current batch is calculated on the basis of other considerations. In an operating furnace depending on the amount of hot metal (pig iron) and slag produced and the chemistry of the feed materials and the products a charge calculation model calculates the amount of

material of different species like iron ore, sinter, pellets, coke, limestone and dolomite to be charged. In our model these species on the basis of their behavior during charging have been classified into two groups, coke and non-coke material. Hence the volume of coke V_c and amount of non-coke material V_{NC} available for the next dumping is known. The total batch volume available is $V_b = V_c + V_{nc}$. The batch volume available may be more than, equal to or less than the required volume ΣV_j. In the first case the stock line after dumping will

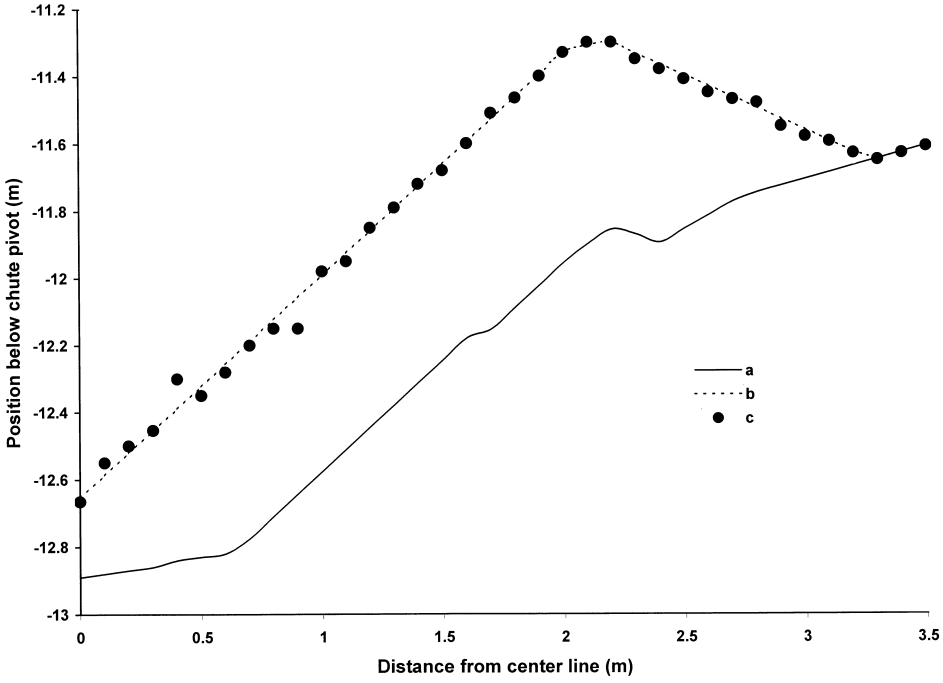

Fig. 10. Model verification on operating furnace for a dump of 26 tons of non-coke material on a coke base line at rings 4 and 5, (a) Base line made of coke, (b) predicted stock line, (c) stock line measured by thermal imaging.

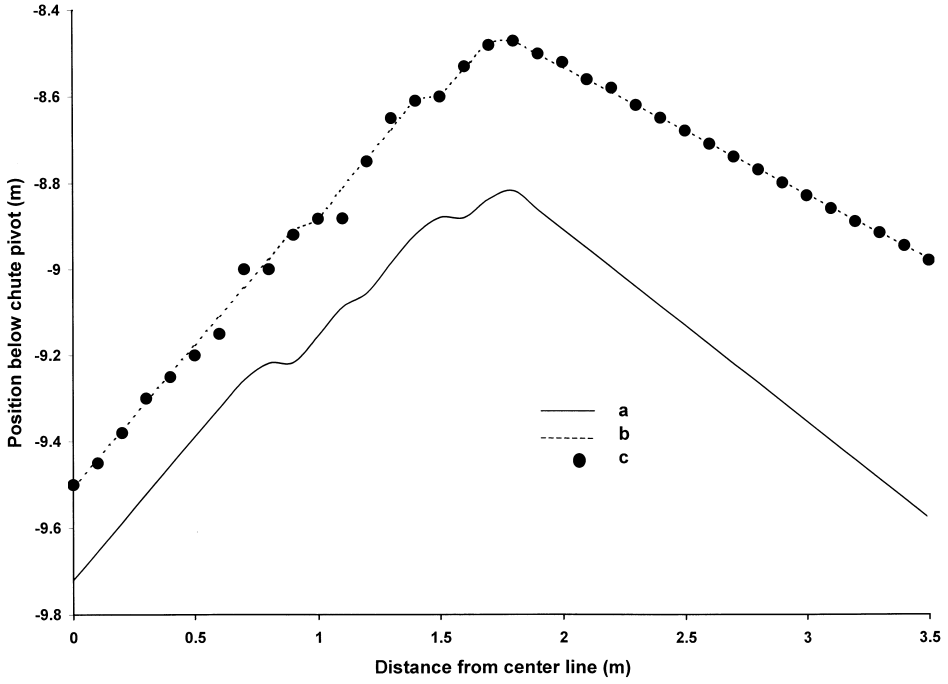

Fig. 11. Model verification on operating furnace for a dump of 9.2 tons of coke material on a non-coke base line at rings 4 and 5, (a) Base line made of non-coke material, (b) predicted stock line, (c) stock line measured by thermal imaging.

overshoot the target. In the second case the stock line can coincide with the target. In the third case the final stock line will lie below the target stock. Where the batch volume and the required volume are same we can achieve the target stock line in the other two cases the objective would be to minimize the difference between the two. This is achieved by minimizing the sum of the squared error between the target profile and the final profile as given in Eqs. (28) and (29). For achieving convergence the following procedure is adopted.

1. Determine the amount of coke and non-coke to be dumped in each of the 11 volumes.The individual dump volumes are determined by apportioning the total batch volume in the same ratio as the required volumes.

$$V_{dj}^{1} = V_{b} \times \frac{V_j}{\Sigma V_j} \tag{32}$$

2. After dumping the volume of material calculated by Eq. (32) in the dumping positions 1–11 the new stock line is calculated by Eqs. (17)–(27).
3. The new stock line is compared with the target stock line and the error at each of the 11 dumping positions are calculated as

$$E_j^{1} = z_j^{t} - z_j^{1} \tag{33}$$

where the superscript 1 denotes that it is the value for the first iteration. The sum of squares of error is given by

$$\text{SSE } E^{1} = \Sigma\left(E_j^{1}\right)^2 \tag{34}$$

Each of the E_j may be positive, zero or negative depending on whether the new stock line at that point is below, coincident or above the target stock line.
4. The dumping is now adjusted according the following sequence. If some of the errors are negative (dumped position above target) and some are positive (dumped position below target), the dumping position corresponding to the most negative error and the most positive error are chosen. From the dumping position corresponding to the most negative error, the dumped volume is reduced by 10% and added to the position corresponding to the most positive error. Then steps 1–3 are carried out and new stock line is determined. The SSE is determined and if the SSE in the second iteration is lower than the first iteration the procedure is continued. This procedure is carried out until all the positive errors are eliminated.
5. When all the errors have become negative or zero the positions corresponding to maximum error and the minimum error are chosen. Again 10% dumped material is transferred from the position of minimum error to the position of maximum error and the new profile and new SSE determined. IF the SSE is reduced then the procedure is continued till there is no change in the SSE.
6. After dealing with the positions corresponding to the maximum error and minimumerror, attention is focussed on the position of second largest error and second smallest error and the same procedure repeated. This method is continued till all the errors are covered. In all cases a search along a path is continued only when the SSE reduces in that direction. Further, if the error at any location is not more than 10 cm then the profile is considered to have achieved the target.
7. When all the errors are negative, meaning the batch volume is more than that required to achieve the target profile, then the same procedure is adopted. In this case the volume dumped in the most negative position is reduced and the volume dumped in the least negative position increased in each iteration till convergence is achieved.

In the procedure adopted the error is minimized at only the 11 dumping positions. Increasing the number of points at which error is minimized could increase accuracy of matching. However, since the required accuracy of 0.01 m in convergence was obtained with 11 points no further attempt was made to increase the number of points used for error minimization.

The optimization procedure outlined was implemented on an operating furnace for several sets of conditions. Two of the typical results are presented in Figs. 12 and 13. In Fig. 12 from an existing 'M' shaped non-coke layer (curve a) the target was to change to a straight-line profile (curve d). It may be noted that only half the profile from the center line ($r = 0$) to wall at $+r$ is shown in the figures. For achieving this a coke dump of 9.2 tons was to be used. The best result achieved by an experienced operator was obtained by dumping this amount of coke in equal volumes in rings 3, 4 and 5 to obtain the profile of curve b. The standard deviation between the target and operator achieved profile was 29 cm. The solid circles in the figure indicate the profile achieved by using the optimization algorithm. The profile achieved is obviously far superior to that obtained by the operator and it is attested to by a lower standard deviation of 0.04 m. The optimized profile was achieved by dumping the material in rings 3, 5 and 6 in the ratio of 2:2:3, respectively.

In the second example illustrated in Fig. 13 the targeted stock line was 'V' shaped (curve c) to be built up from a 'M' shaped base stock line (curve a) of non-coke material. The best profile achieved by the operator (curve b) by dumping the coke on rings 3,4 and 5 in

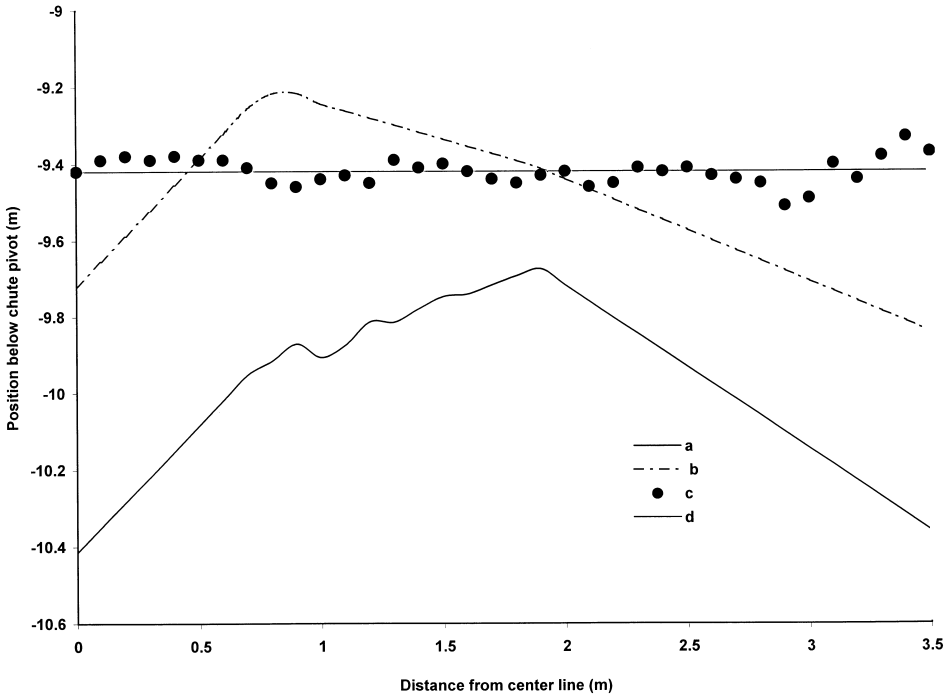

Fig. 12. Transition from an existing 'M' shaped profile made up of non-coke material to a straight line profile by a dump of 9.2 tons of coke material, (a) Base line made of coke, (b) best profile obtained manually by an experienced operator by dumping on rings 4, 5 and 6 in equal volumes, (c) profile obtained by the optimization strategy by dumping on rings 3,5 and 6 in the ratio of 2:2:3, (d) target straight line profile.

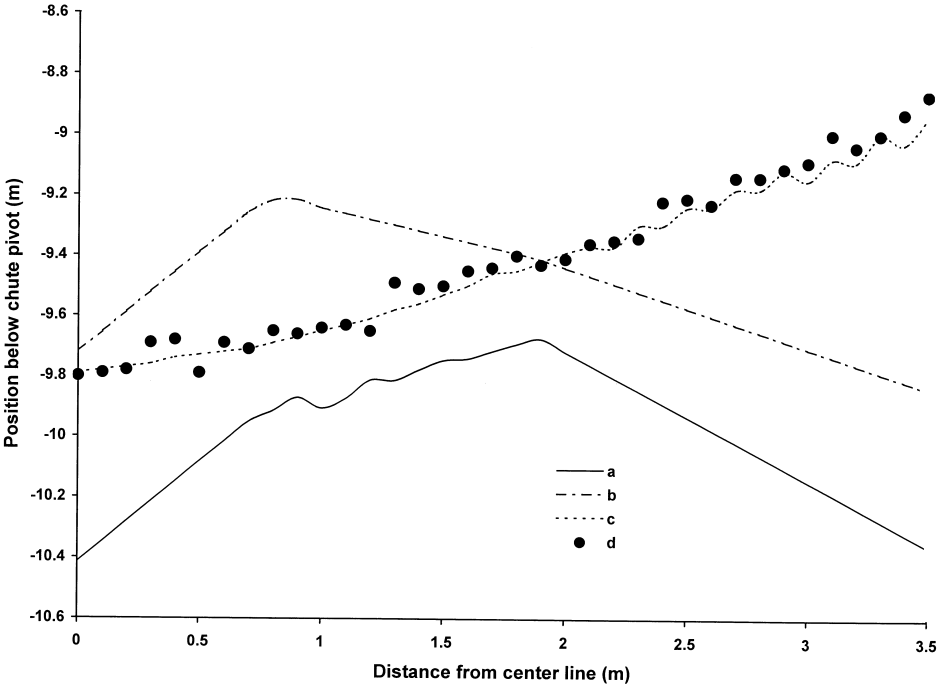

Fig. 13. Transition from an existing 'M' shaped profile made up of non-coke material to a 'V' profile by a dump of 9.2 tons of coke material,(a) base line made of coke, (b) best profile obtained manually by an experienced operator by dumping on rings 3, 4 and 5 in equal volumes, (c) target 'V' shaped profile, (d) profile obtained by the optimization strategy by dumping on rings 3,7 and 8 in the ratio of 2:2:4.

equal volumes had a standard deviation of 27 cm. As compared to this the optimized dumping recommended dump sequence in rings 3,7 and 8 in the ratio 2:2:4, respectively. The resulting dump achieved almost perfect target having a standard deviation of 0.03.

8.2. Control implementation

The model based control developed in this work has been implemented as the supervisory system over the existing PLC based regulatory controls of the Paul–Wurth bell-less top charging system. The structure of the control system is illustrated in Fig. 14. The model based predictive controller obtains information regarding the current stock line profile from the infrared imaging system. The burden descent rate is obtained from the stock rod instrumentation system. The charge calculation model, which is also in the supervisory layer, provides the quantity of the next batch and the constituents making it up. The target profile is entered by the plant engineer or is chosen from one of the stored profiles. The control model determines by the use of the model optimization algorithm the location of the rings on which dumping is to take place and the quantity to be dumped on each ring. The calculated values of the chute angle are down loaded to the PLC system and acts as set points for the control. The PLC system works with hydraulic actuators as the final control elements for adjusting the chute angle setting and the gate valve opening. The control system basically operates in the servo mode. The hydraulic actuator together with the chute mechanism was modeled using frequency response testing. The iterative least square method proposed by Sanathanan and Koerner [11] was used to obtain the process model . The polynomial model could be represented by the equation,

$$\frac{Y}{X} = \frac{0.1906}{0.00129s^3 + 0.017s^2 + 0.14s + 1} \tag{35}$$

where

Y = chute angular displacement radian
X = input current, mA
S = Laplace operator

The Bode diagram of the system is shown in Fig. 15. The three roots of the characteristic equation are -10.05, -1.56 ± 8.64 i. From the open loop root locus shown in Fig. 16 it is clear that the pair of complex roots lying very near to the imaginary axis is a source of potential instability in the system. The open loop system has a gain margin of 12.9 dB at the critical frequency $\omega_c = 10.4$ rad/s. In the Nyquist diagram shown in Fig. 17 the point $(-1,0)$ is encircled once with unity feed back. Simulation using MATLAB showed that the system could become unstable with even moderate values of the proportional gain. Introduction of integral action made the situation worse. Even with very high values of integral time the system became unstable. Hence it was not possible to use integral action. The choice was therefore Proportional plus Derivative control. As discussed earlier the control system has the basic function of Servo Control to change the chute settings according to the supervisory level commands. On an average the chute position has to be changed more than 100 times in

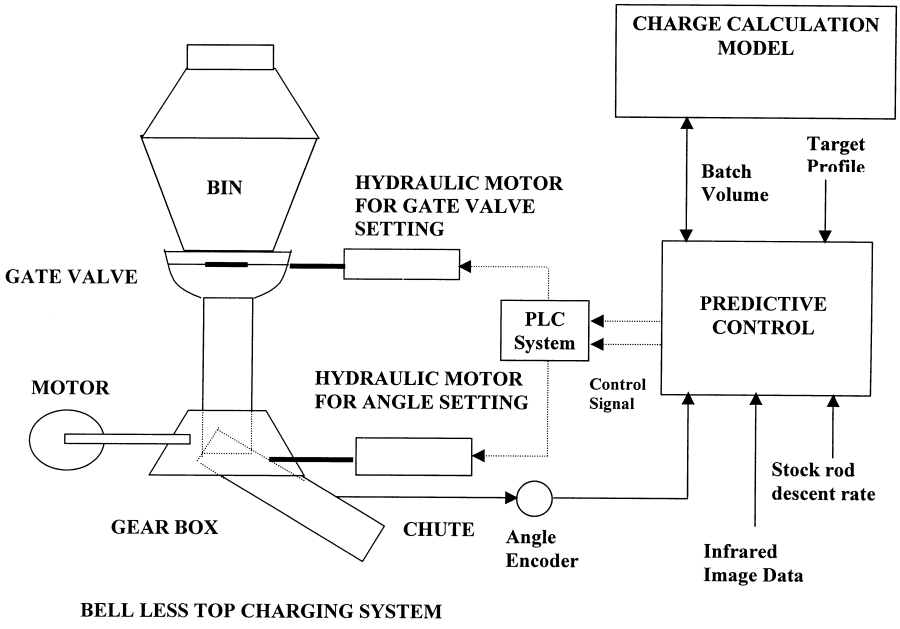

Fig. 14. Schematic diagram of the predictive control system for the bell-less top charging system.

a day. To minimize the wear and tear of the heavy mechanisms involved it was decided that the normal tuning for a quarter decay ratio is not applicable. Instead a dead beat response without any overshoot and oscillation were targeted. The system was simulated in the MATLAB environment and the appropriate values of the Proportional Gain and Derivative time were determined to give the best response from the minimum

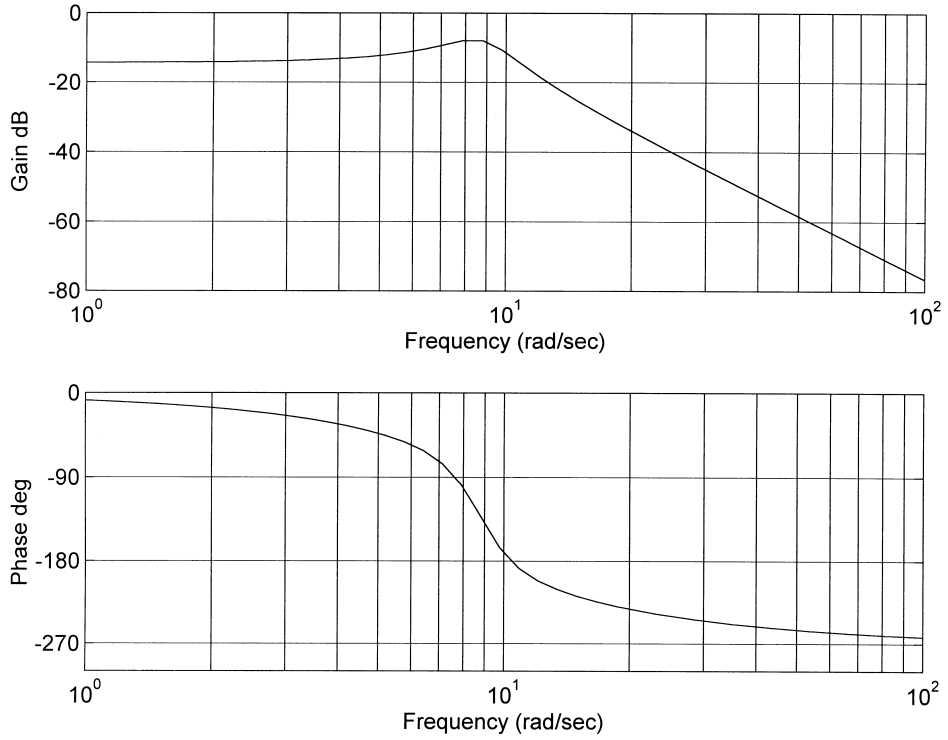

Fig. 15. Open loop Bode diagram of the hydraulic control system.

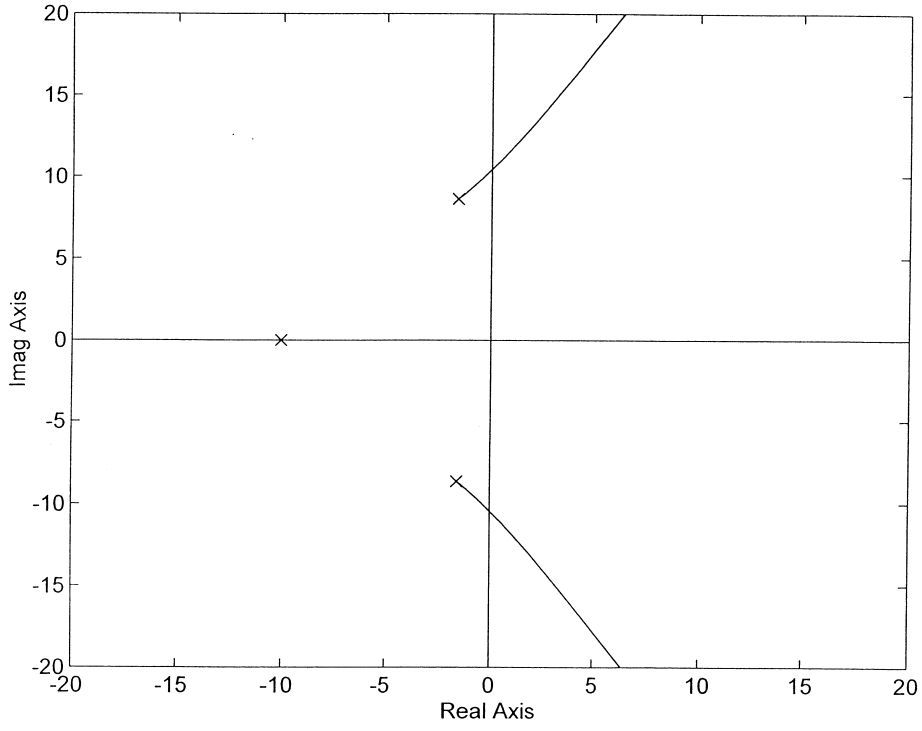

Fig. 16. Root locus diagram of the hydraulic servo control system under proportional control.

integral error sense, subject to zero overshoot. The best response obtained is shown in Fig. 18 for a value of $K_c = 0.2$ and $T_D = 2.5$. Since integral action was not present some offset was present but this could be tolerated within the accuracy desired.

The model based predictive control scheme has been implemented in an operating furnace. With the predictive control the furnace has been operating in a much smoother manner. Furnace hanging, which used to occur on the average 1.8 times per day, has been practically

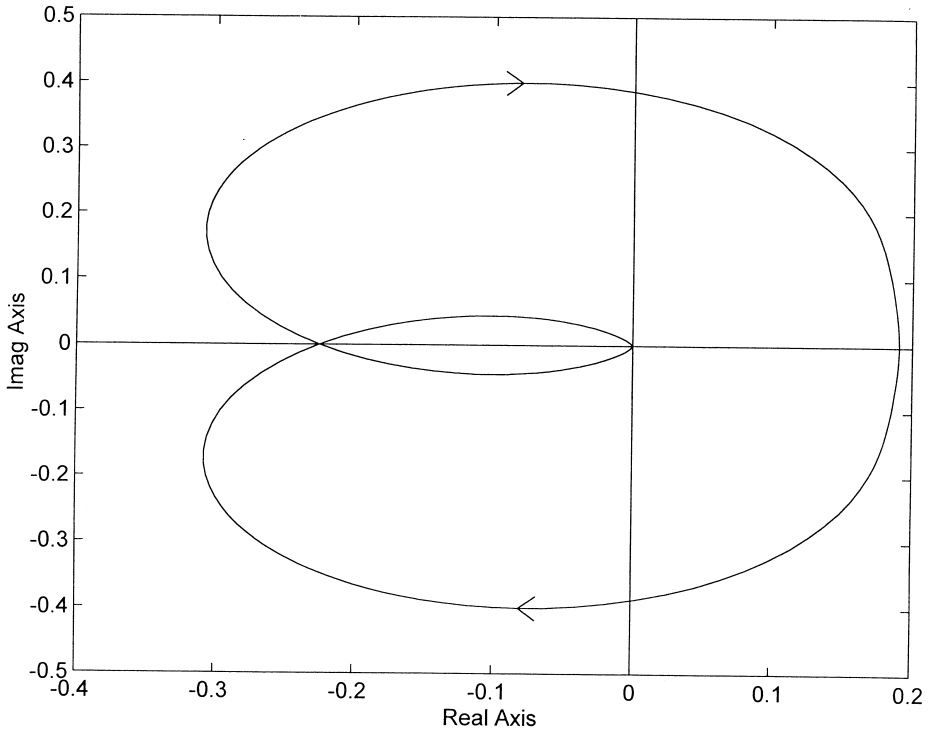

Fig. 17. Nyquist diagram of the system under proportional control.

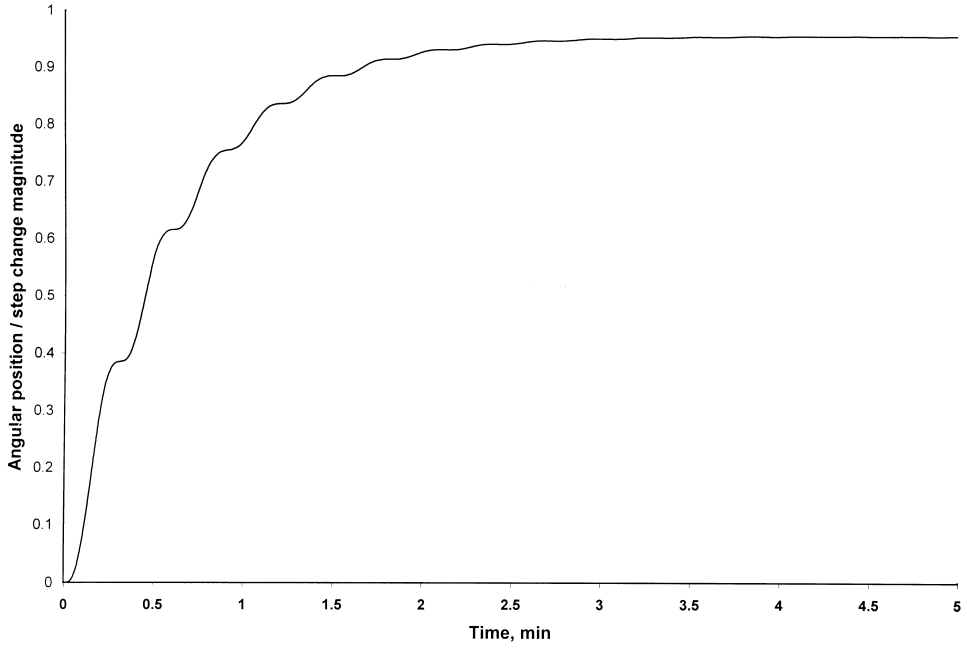

Fig. 18. Step response of the system under proportional-derivative control with $K_c = 0.2$ and $T_D = 2.5$.

eliminated. The stock rod descend rate has increased by an average of 2.5%. Since the stock rod descend rate signifies the rate of material movement down the furnace there is a corresponding increase in the furnace productivity. This has resulted in a productivity improvement of the order of 75 ton of hot metal per day.

9. Conclusions

A mathematical model for the burden trajectory and stock line geometry derived from simple mechanistic considerations has been found to work extremely well in both cold and hot runs. An optimization algorithm based on the model has been effectively used for the predictive control of the charging system. The model based predictive control has resulted in smoother furnace operation and an improvement in productivity of the order of 2.5%.

Acknowledgements

The authors acknowledge the facilities made available by Steel Authority of India Ltd., for conducting the study. One of the authors (KMR) acknowledges the funding and permission provided by SAIL for his graduate studies.

References

[1] Y. Shimonura, K. Nishikawa, S. Arino, T. Katayama, Y. Hida, Correlation of cohesive zone with charge layers at the furnace top, Tatsu-To-Hagane 62 (1976) 547.
[2] Y. Okumo, Development of a mathematical model for burden distribution in a blast furnace, in: 44th Iron Making Conference, Detroit, Proc. 1985, pp. 543–552.
[3] P.D. Burk, J.M. Burgess, A coupled gas and solid flow heat transfer & chemical reaction model, in: Iron Making Conference, Chicago, Proc. 1989, pp. 773–781.
[4] K. Yoshimasa, T. Jimbo, T. Sakai, Development of simulation model for burden distribution at blast furnace top, Trans. ISIJ. 23 (1045) 1983.
[5] M. Sakai, K. Ono, A. Suzuki, Y. Okuno, K. Yoshizawa, Burden descent characteristics in blast furnaces, Tatsu-To-Hagane 62 (1976) 557–565.
[6] Y. Kajimasa, T. Jimbo, A. Komatani, Y. Shimoda, Application of simulation model for burden distribution to actual operation, Trans. ISIJ. 22 (1982) 243–250.
[7] K. Yoshimasa, T. Jimbo, T. Joko, Y. Aminago, T. Inada, Investigations of bell-less charging based on full scale model experiments, Trans. ISIJ. 24 (1984) 799.
[8] N. Standish, Principles of burdening and bell-less charging, Nimaroo Publishers, Wolloongong, Australia, 1989.
[9] T. Nagai, Control of Burden Distribution by Bell-Less Top System at Chiba Works, Mc Master symposium on optimum burden distribution in blast furnaces, May, 1978, pp. 13.1–13.27.
[10] B.Y. Hay, A.W. Kay, C.W. Thom, Burden Distribution with Single Lock Hopper Bell-Less Top, Report published by Stelco Inc., Hamilton, Ontario, Canada, 1985, p. 184.
[11] C.K. Sanathanan, J. Koerner, Complex function synthesis as a ratio of two complex polynomials, IEEE Trans. Auto. Contr. AC-8 (1963) 37.